

# A complete digital optics applied to digital holographic microscopy: application to chromatic aberration compensation

Tristan Colomb<sup>a,b</sup>, Florian Charrière<sup>b</sup>, Jonas Kühn<sup>b</sup>, Frédéric Montfort<sup>c</sup> and Christian Depeursinge<sup>b</sup>

<sup>a</sup>Centre de Neurosciences Psychiatriques, Département de psychiatrie DP-CHUV, Site de Cery, 1008 Prilly-Lausanne, Switzerland;

<sup>b</sup>Ecole polytechnique fédérale de Lausanne, Institute of imaging and applied optics, CH-1015 Lausanne, Switzerland;

<sup>c</sup>Lyncée Tec SA, PSE-A, CH-1015 Lausanne

## ABSTRACT

In optics, optical elements are used to transform, to filter or to process physical wavefronts in order to magnify images, compensate for aberration or to suppress unwanted diffracted order for example. Because digital holography provides numerical wavefronts, we developed a digital optics, involving numerical elements such as numerical lenses and pinholes, to mimic numerically what is usually done physically, with the advantage to be able to define any shape for these elements and to place them everywhere without obstruction problems. We demonstrate that automatic and non-automatic procedures allow diffracted order or parasitic interferences filtering, compensation for aberration and image distortion, and control of position and magnification of reconstructed wavefront. We apply this digital optics to compensate for chromatic aberration in multi-wavelength holography in order to have perfect superposition between wavefronts reconstructed from digital hologram recorded with different wavelengths. This has a great importance for synthetic wavelength digital holography or tomographic digital holography that use multiple wavelengths.

**Keywords:** Digital holography, aberration compensation, microscopy

## 1. INTRODUCTION

Digital holographic microscopes (DHM) allow retrieving quantitative information of object wavefront by the numerical reconstruction of its amplitude and phase from a digital hologram recorded by a CCD or CMOS camera.<sup>1-3</sup> The digitalization of the hologram allows to store a numerical wavefront in the hologram plane, and therefore it allows defining a numerical optics to perform optical processing of this stored wavefront. Indeed, the object wavefront in the hologram plane can be propagated at any distances<sup>4</sup> and numerical pinholes,<sup>5</sup> numerical lenses,<sup>6,7</sup> or holograms<sup>8</sup> can be used to perform spatial frequency filtering, image shifting, magnification, or compensation of distortion or phase aberrations introduced by the real optical elements in the setup.

Using multi-wavelengths digital holography allows to perform color holography,<sup>9-13</sup> synthetic wavelength digital holography<sup>14,15</sup> or tomography.<sup>16-19</sup> Usually, the multi-wavelengths DHM setups acquire different off-axis holograms with different wavelengths, but with the same angle between the object and reference waves. Because the fringe pattern frequency depends on the angle and the wavelength, different spatial frequency filters have to be defined in the Fourier plane of the hologram.<sup>3</sup> Furthermore, if the optics are not totally achromatic, different problems could occur. First the reconstruction distances for each hologram change, and different image shift or/and magnification could occur in the reconstruction plane. We present here a method to compute automatically the spatial frequency filter for the different holograms from the manual definition of a first one; and we use the concept of numerical optics to obtain reconstructed images with the same magnification and position.

---

Further author information: (Send correspondence to Tristan Colomb)  
E-mail: tristan.colomb@a3.epf.ch, Telephone: +41 21 693 37 42

## 2. MULTI-WAVELENGTHS SETUP

The setup is based on a classical Mach-Zehnder off-axis holographic interferometer (Fig. 1). The light source is generated by an argon ion plasma laser (Coherent Innova 200) pumping a modelocked Ti:S laser system (Coherent Mira 900). The beam is then amplified by a regenerative amplifier (Coherent RegA 9000) and finally extended in wavelength with a tunable optical parametric amplifier (Coherent OPA 9400). The beam coming from the optical parametric amplifier (OPA) is split. On one side, the object beam  $O_{\lambda_i}$  illuminates the sample through the microscope objective (MO, focal length 18.4 mm, NA=0.15, magnification  $\sim 10\times$ ) and the back scattered field, collected by the MO, interferes on the CCD with the reference beam  $R_{\lambda_i}$  to produce a hologram for the different wavelength  $\lambda_i$ :

$$I_{H,i}(x, y) = |R_{\lambda_i}|^2 + |O_{\lambda_i}|^2 + R_{\lambda_i} O_{\lambda_i}^* + R_{\lambda_i}^* O_{\lambda_i}. \quad (1)$$

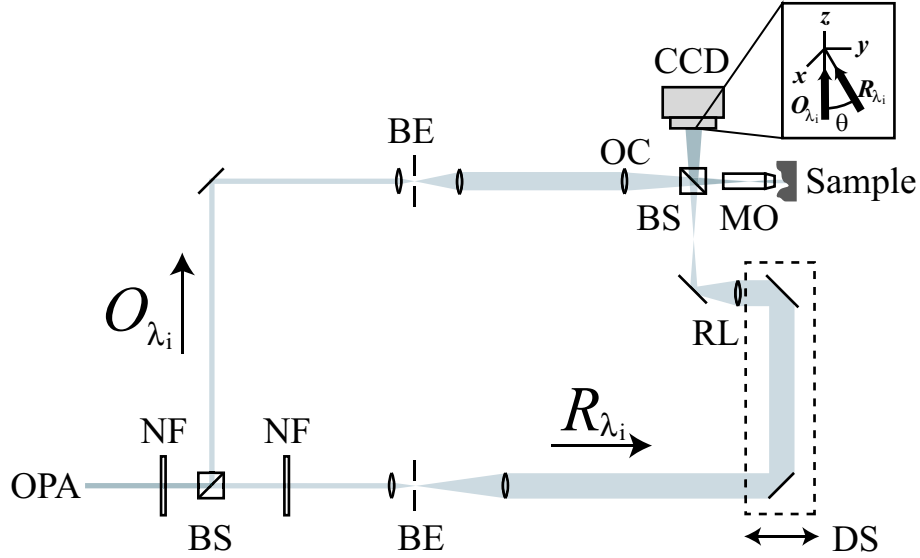


**Figure 1.** Experimental setup.  $O_{\lambda_i}$ : object wave at  $\lambda_i$ ,  $R_{\lambda_i}$ : reference wave at  $\lambda_i$ , OPA: adjustable wavelength laser, NF: neutral filter, BS: beam splitters, BE: Beam Expander, MO: Microscope Objective, OC: Object Beam Condenser, RL: Reference Lens, CCD: Charged Coupled Device Camera, DS: Delay System.

In our case, the holograms are recorded in an off-axis geometry, meaning that a small angle  $\theta$  is introduced between both waves. As the coherence length of the OPA beam is short (about  $60\mu\text{m}$ ), the optical length of the reference beam is adjusted to the one of the object with a delay system (DS). Two more lenses are used: one is the object beam condenser (OC) that focuses the object beam at the back focal length of the microscope objective in order to have a collimated beam illuminating the sample, and the second is the reference lens (RL) that curves the reference beam to match approximatively the curvature introduced by the microscope objective on the object beam in the CCD plane. This curvature matching is approximative and does not require an exact and delicate adjustment of RL position, because the residual curvature difference can be easily compensated numerically as presented in details in Refs. 6, 7. It is to note that the image of the specimen through the MO is not focused on the CCD camera. This setup was used to perform tomographic imaging, computed from a sequence of 20 holograms recorded with 20 different wavelengths without moving any part of the setup,<sup>19</sup> excepting the DS to compensate for dispersion between each wavelength and NF to adjust the beams intensities.

## 3. AUTOMATIC SPATIAL FREQUENCY FILTERING

The first step of the reconstruction procedure consists to apply a spatial frequency filter on the spectrum [Fig. 2(b)] for the different holograms [Fig. 2(a)], in order to propagate only the virtual images ( $R_{\lambda_i}^* O_{\lambda_i}$ ) of Eq. 2. The filtered digital holograms are computed as:

$$I_{H,i}^F(k, l) = \text{FFT}^{-1} [\text{FFT}(I_{H,i})P_i(\nu_k, \nu_l)], \quad (2)$$

where  $P_i(\nu_k, \nu_l)$  is a mask defining the spatial filtering, that can be seen as a numerical pinhole for the wavelength  $\lambda_i$ ; and  $\nu_k, \nu_l$  are the spatial frequencies coordinates. Let us take a first hologram [Fig. 2(a)] corresponding to the smaller wavelength  $\lambda_{min}$ . The spectrum of this hologram [Fig. 2(b)] is filtered manually as shown in Fig. 3(a), suppressing real image, zero order ( $|\mathbf{R}_{\lambda_i}|^2 + |\mathbf{O}_{\lambda_i}|^2$ ) and parasitic interferences.<sup>3</sup> Then for each other wavelength, the digital spatial filter is computed automatically by a simple procedure. The carrier frequency of the fringe pattern at  $f_{\lambda_i}$  and in the x-direction depends on the angle  $\theta$  between the reference and the object wave (for y-direction the same demonstration can be done):

$$f_{\lambda_i} = \frac{2\pi}{\lambda_i} \cos \theta. \quad (3)$$

Furthermore, the highest recorded frequencies of the object follow the same equation. Therefore, because the angle is constant for each wavelength, the automatic filters are computed automatically from the initial one, by scaling  $P_{\lambda_{min}}(\nu_k, \nu_l)$  by:

$$s_{\lambda_i} = \frac{f_{\lambda_i}}{f_{\lambda_{min}}} = \frac{\lambda_{min}}{\lambda_i}. \quad (4)$$

In Fig. 3(b,c),  $P_i(\nu_k, \nu_l)$  are scaled respectively by a factor  $s_{586.8} = 0.818$  and  $s_{700} = 0.686$  and then centered on the spectrum image (the frequencies outside the white rectangle are filtered).

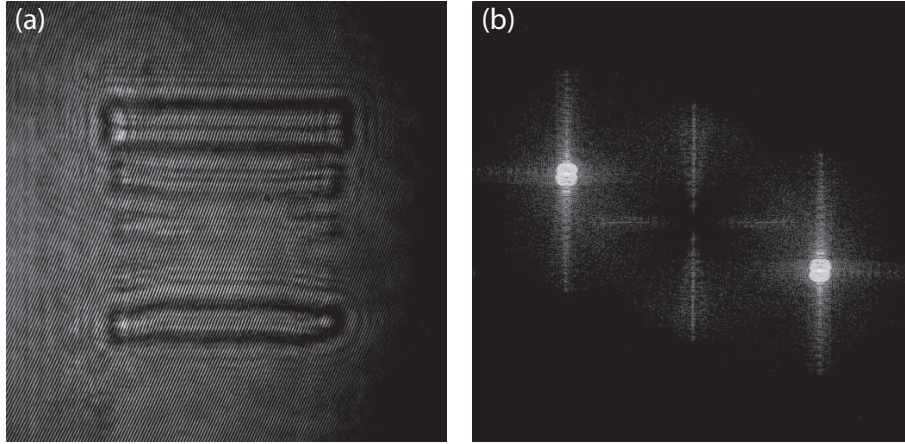


**Figure 2.** (a) Hologram and (b) spectrum obtained at  $\lambda = 480\text{nm}$  for a custom test target.

#### 4. RECONSTRUCTION AND CHROMATIC ABERRATION COMPENSATION

The reconstruction of the object wavefront is computed with the convolution formalism of the Fresnel propagation:<sup>7</sup>

$$\Psi_{CF,i}(m, n) = \Gamma_i^I(m, n) \cdot A_i \cdot \text{FFT}^{-1} \left\{ \text{FFT} \left[ \Gamma_i^H(k, l) I_{H,i}^F(k, l) \right] \cdot \exp \left[ -i\pi\lambda_i d_i (\nu_k^2 + \nu_l^2) \right] \right\}, \quad (5)$$

where, FFT is the Fast Fourier Transform;  $m, n, k, l$  are integers ( $-N/2 < m, n, k, l \leq N/2$ );  $d_i$ , the reconstruction distance for wavelength  $\lambda_i$ ;  $A = \exp(i2\pi d_i / \lambda_i) / (i\lambda_i d_i)$ ;  $\nu_k = k / (N\Delta x)$ ,  $\nu_l = l / (N\Delta y)$  are the spatial frequencies coordinates;  $\Delta x$  and  $\Delta y$  are the pixel sizes of the CCD camera; and  $\Gamma_i^I$  and  $\Gamma_i^H$  are numerical parametric lenses (NPLs) placed respectively in the image and hologram plane.

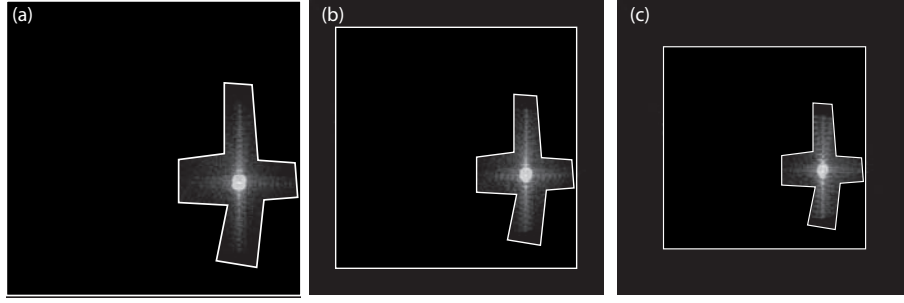


**Figure 3.** Filtered spectrums for holograms recorded at (a) 480nm, (b) 586.8nm and (c) 700nm. The filters for (b) and (c) are computed from the filter of (a).

The NPLs  $\Gamma_i^I$  and  $\Gamma_i^H$  are used to compensate for phase aberration by using polynomial fitting on flat areas of the specimen<sup>6,7</sup> or by using a reference hologram.<sup>8</sup> The reconstructed images for two different wavelengths are presented in Fig. 4. Due to chromatic aberration of the microscope objective, the reconstruction distances and the magnifications of the specimen are different for each wavelength as seen on Fig. 4(a-d).

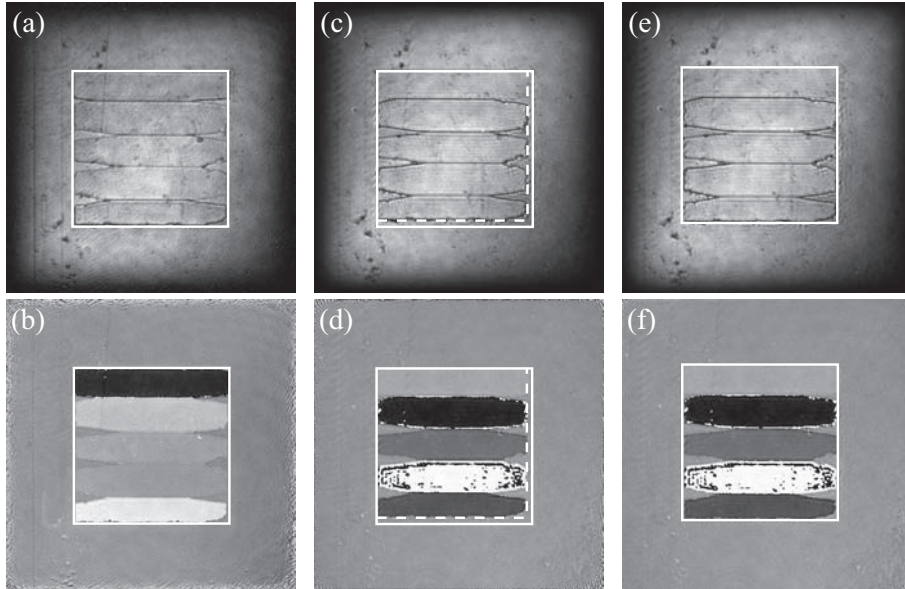


**Figure 4.** The amplitude and the phase reconstructions are presented respectively in the first and second line. The reconstructions are done from a hologram recorded with  $\lambda = 480\text{nm}$ ,  $d_{480} = -2.99\text{cm}$  (a,b) and  $\lambda_2 = 700\text{nm}$ ,  $d_{700} = 0.01\text{cm}$  (c-f). The white rectangle defines the reference size. The white dashed rectangle defines the size of the same object without performing magnification. (e,f) are reconstructed from the same hologram as (b,c) after performing a magnification procedure  $M = 1.0038$  defined by the quotient of the rectangle sizes

#### 4.1. Magnification

The magnification difference for the different wavelength is compensated by using other NPLs  $\Gamma_i^{H,M}$  and  $\Gamma_i^{I,M}$ . First of all, a first reconstruction serves as size reference [here Fig. 4(a,b)]. Then, for each wavelength, the desired magnification  $M_i$  is determined by computed with the quotient of the white rectangles sizes defined in Fig. 4(a-d). The principle now is to compute a NPL in the hologram plane that has the correct focal  $f_i$  to produce the desired magnification  $M_i$ .

The Magnification NPL can be described by a thin lens transmittance:<sup>20</sup>

$$\Gamma_i^{H,M}(m, n) = \exp \left[ i \frac{2\pi}{\lambda_i} \frac{1}{2f_i} (m^2 \Delta x^2 + n^2 \Delta y^2) \right]. \quad (6)$$

Let us defining  $H$  the hologram plane where the NPL with focal distance  $f_i$  is placed,  $I$  the original image plane defining by the reconstruction distance  $d_i$  (position of the reconstructed virtual image) and  $I'$  the final image plane defined by the reconstruction distance  $d'_i$ . From these definitions, the real object (having the same size as the virtual image) is at a distance  $-d_i$  from the hologram plane. The magnification  $M_i$  for the wavelength  $\lambda_i$  is also calculated from the real object and image distances:

$$M_i = -\frac{d'_i}{-d_i} = \frac{d'_i}{d_i}. \quad (7)$$

The new reconstruction distance is

$$d'_i = M_i d_i. \quad (8)$$

Finally, the focal of the magnification lens is easily computed with the lens equation and introducing Eq. 8

$$\frac{1}{f_i} = \frac{1}{-d_i} + \frac{1}{d'_i} = \frac{1}{-d_i} + \frac{1}{M_i d_i} \quad (9)$$

Obviously, the phase curvature introduced in the hologram plane by the NPL have to be compensated in the new image plane  $I'$ . The predicted compensation for the Magnification NPL in the image plane is

$$\Gamma_i^{I,M}(m, n) = \exp \left[ i \frac{2\pi}{\lambda_i} \frac{1}{2(f_i - d'_i)} (m^2 \Delta x^2 + n^2 \Delta y^2) \right]. \quad (10)$$

The use of these NPL allows to reconstruct specimen with the same magnification as presented in Fig. 4(e,f).

## 4.2. Shift

Because the magnification is done from the center to the edge of the image, or due to a modification of the pointing of the laser for the different wavelengths, the reconstructed images could be slightly shifted in the image plane. To compensate for these effect, a manual shift is developed. For this purpose, we define the Shifting NPL's  $\Gamma_S^{H,Sh}$  and  $\Gamma_S^{I,Sh}$ . The principle of the procedure have three steps. First of all, the operator draws two points defining the shift to achieve [arrows on Fig. 5(a)]. The second step consists in computing the parameters  $S_x$  and  $S_y$  of

$$\Gamma_S^{H,Sh}(\mathbf{x}) = \exp \left[ i \frac{2\pi}{\lambda} \hat{\mathbf{S}} \mathbf{x} \right] = \exp \left[ i \frac{2\pi}{\lambda} (S_x m \Delta x + S_y n \Delta y) \right]. \quad (11)$$

These parameters can be easily computed by considering Fig. 5(c). Let us define the chosen shift in the two directions:

$$\Delta S_j = N_{Sj} \Delta j, \quad (12)$$

where  $j = x, y$ ,  $N_{Sj}$  is the number of pixels to shift in the  $j$ -direction. The Shifting NPL is written as:

$$\Gamma_S^{H,Sh}(\mathbf{x}) = \exp \left[ i \frac{2\pi}{\lambda} \hat{\mathbf{S}} \mathbf{x} \right] = \exp \left[ i \frac{2\pi}{\lambda} (S_x m \Delta x + S_y n \Delta y) \right], \quad (13)$$

where  $\hat{\mathbf{S}}$  is the unit shift vector. The components of the vector  $\hat{\mathbf{S}}$  are:

$$S_j = \sin(\theta_j) = \sin \left[ \arctan \left( \frac{\Delta S_j}{d} \right) \right]. \quad (14)$$

Obviously this shift introduced in the hologram plane produces a tilt in the image plane that should be compensated. We introduce therefore a predicted compensating Shifting NPL in the image plane defined as:

$$\Gamma_S^{I,Sh}(m, n) = \exp \left[ -i \frac{2\pi}{\lambda} (S_x m \Delta x + S_y n \Delta y) \right], \quad (15)$$

Figures 5(b) presents the shifted reconstructed phase.

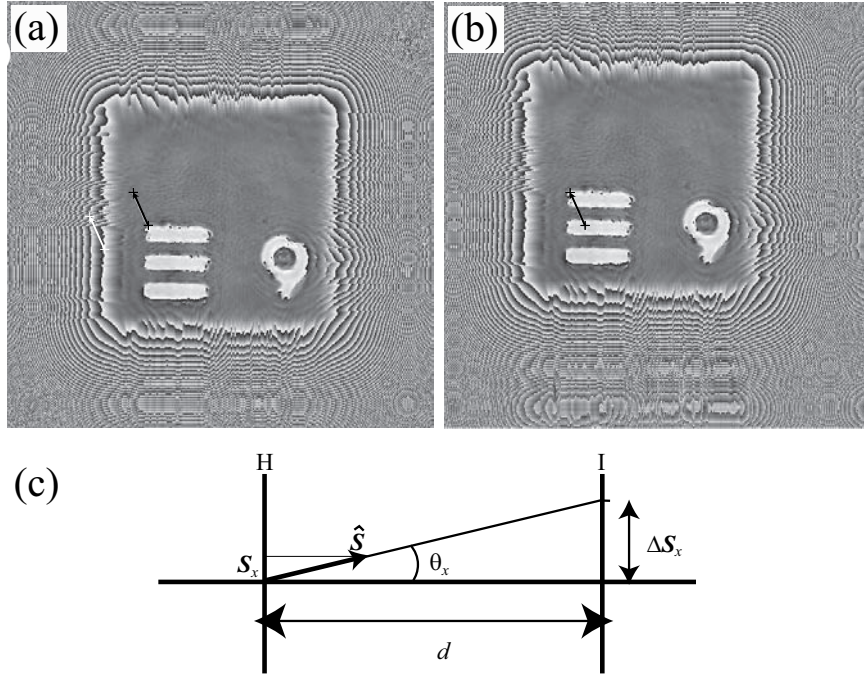


**Figure 5.** Shifting procedure. (a) and (b) are respectively the phase reconstructions before and after shift compensation. The arrows define the chosen translation of the ROI. (c) Shift principle: H, hologram plane; I, image plane;  $\Delta S_x$ , chosen shift in the direction  $x$ ;  $d$ , reconstruction distance and  $\theta_x$ , shifting angle.

## 5. RESULTS

The automatic filtering and the magnification procedure are applied in the context of sub-micron optical tomography by multiple wavelength DHM. The principle consists in recording several holograms with different wavelengths (typically 20 holograms with wavelengths between 480 nm and 700 nm) with a reflection DHM. The reconstruction of these holograms and their processing allows tomographic imaging.<sup>19</sup> The Figure 6 compares the mean amplitude computed from the 20 holograms (a,b) and the mapping of it on the three-dimensional topography of the specimen (c,d) when the magnification is applied to superimposed all 20 reconstructed images (b,d) or not (a,c). We can see clearly that (a) is blurred whereas (b) is not. The improvement of the method is also visible for (d) where the noise on the specimen edges is clearly diminished.

## 6. CONCLUSION

In this paper we present a digital optics applied in multi-wavelengths digital holography, allowing to compensate for magnification mismatch due to chromatic aberrations, in addition with the compensation for phase aberration and/or image distortion, by the use of numerical lenses. Furthermore, we present a simple automatic procedure to compute numerical spatial frequency filter from a calibrated filter obtained for a single wavelength. Many application of multi-wavelength digital holography such as tomography, color holography, could take in account these results to increase the quality of the superposition of the reconstructed wavefront and the cost of the setup could decreased because non-achromatic optics can be used.

## Acknowledgments

The development of the technology has been supported by Swiss government through the research grant 205320-103885/1 from the Swiss National Science Foundation and the research grant 7152.1 from the Innovation Promotion Agency (KTI/CTI). The author thanks the people at Lyncee Tec SA ([www.lynceetec.com](http://www.lynceetec.com)) for their collaboration and the fruitful discussions.

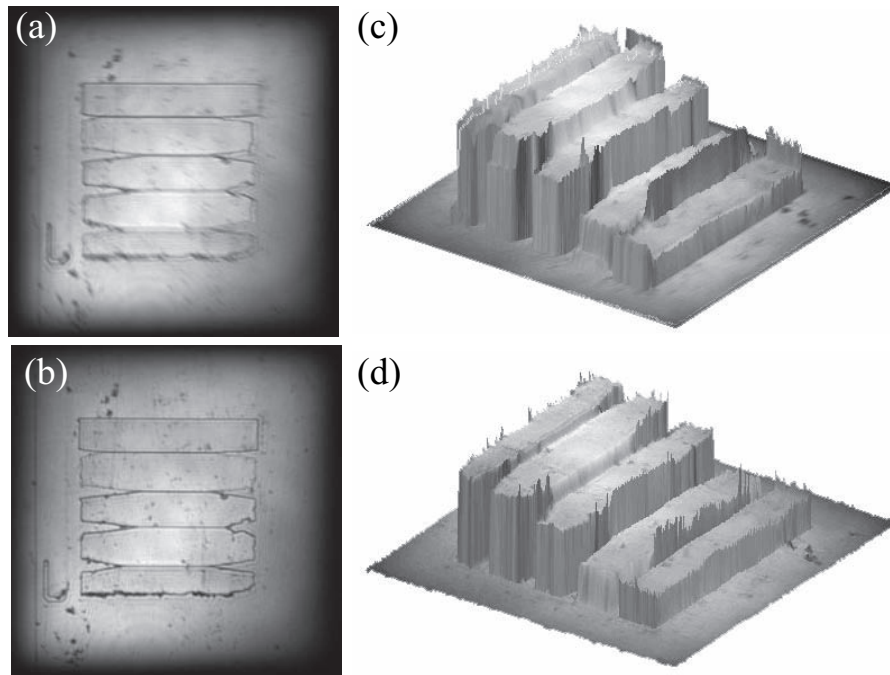


**Figure 6.** (a,b) Mean amplitude reconstructed from 20 holograms recorded with different wavelengths and (c,d) mapping of it on the three-dimensional topography of the specimen. (b,d) are processed with shift and magnification compensation.

## REFERENCES

1. U. Schnars and W. Jüptner, "Direct recording of holograms by a ccd target and numerical reconstruction," *Appl. Opt.* **33**(2), pp. 179–181, 1994.
2. E. Cucho, F. Bevilacqua, and C. Depeursinge, "Digital holography for quantitative phase-contrast imaging," *Opt. Lett.* **24**(5), pp. 291–293, 1999.
3. E. Cucho, P. Marquet, and C. Depeursinge, "Simultaneous amplitude-contrast and quantitative phase-contrast microscopy by numerical reconstruction of fresnel off-axis holograms," *Appl. Opt.* **38**(34), pp. 6994–7001, 1999.
4. P. Ferraro, S. Grilli, D. Alfieri, S. D. Nicola, A. Finizio, G. Pierattini, B. Javidi, G. Coppola, and V. Striano, "Extended focused image in microscopy by digital holography," *Opt. Express* **13**(18), pp. 6738–6749, 2005.
5. E. Cucho, P. Marquet, and C. Depeursinge, "Spatial filtering for zero-order and twin-image elimination in digital off-axis holography," *Appl. Opt.* **39**(23), pp. 4070–4075, 2000.
6. T. Colomb, E. Cucho, F. Charrière, J. Kühn, N. Aspert, F. Montfort, P. Marquet, and C. Depeursinge, "Automatic procedure for aberration compensation in digital holographic microscopy and applications to specimen shape compensation," *Appl. Opt.* **45**(5), pp. 851–863, 2006.
7. T. Colomb, F. Montfort, J. Kühn, N. Aspert, E. Cucho, A. Marian, F. Charrière, S. Bourquin, P. Marquet, and C. Depeursinge, "Numerical parametric lens for shifting, magnification and complete aberration compensation in digital holographic microscopy," *J. Opt. Soc. Am. A* **23**(12), pp. 3177–3190, 2006.
8. T. Colomb, J. Kühn, F. Charrière, C. Depeursinge, P. Marquet, and N. Aspert, "Total aberrations compensation in digital holographic microscopy with a reference conjugated hologram," *Opt. Express* **14**(10), pp. 4300–4306, 2006.
9. J. Kato, I. Yamaguchi, and T. Matsumura, "Multicolor digital holography with an achromatic phase shifter," *Opt. Lett.* **27**(16), pp. 1403–1405, 2002.
10. I. Yamaguchi, T. Matsumura, and J. Kato, "Phase-shifting color digital holography," *Opt. Lett.* **27**(13), pp. 1108–1110, 2002.

11. P. Almoró, M. Cadatal, W. Garcia, and C. Saloma, "Pulsed full-color digital holography with a hydrogen raman shifter," *Appl. Opt.* **43**(11), pp. 2267–2271, 2004.
12. B. Javidi, P. Ferraro, S.-H. Hong, S. D. Nicola, A. Finizio, D. Alfieri, and G. Pierattini, "Three-dimensional image fusion by use of multiwavelength digital holography," *Opt. Lett.* **30**(2), pp. 144–146, 2005.
13. B. Javidi, C. M. Do, S.-H. Hong, and T. Nomura, "Multi-spectral holographic three-dimensional image fusion using discrete wavelet transform," *Journal of the Display Technology* **2**(4), pp. 411–417, 2006.
14. J. Gass, A. Dakoff, and M. K. Kim, "Phase imaging without 2 pi ambiguity by multiwavelength digital holography," *Opt. Lett.* **28**(13), pp. 1141–1143, 2003.
15. D. Parshall and M. Kim, "Digital holographic microscopy with dual wavelength phase unwrapping," *Appl. Opt.* **45**(3), pp. 451–459, 2006.
16. M. K. Kim, "Wavelength-scanning digital interference holography for optical section imaging," *Opt. Lett.* **24**(23), pp. 1693–1695, 1999.
17. M. K. Kim, "Tomographic three-dimensional imaging of a biological specimen using wavelength-scanning digital interference holography," *Opt. Express* **7**(9), pp. 305–310, 2000.
18. L. Yu and M. K. Kim, "Wavelength scanning digital interference holography for variable tomographic scanning," *Opt. Express* **13**(15), pp. 5621 – 5627, 2005.
19. F. Montfort, T. Colomb, F. Charrière, J. Kühn, P. Marquet, E. Cuche, S. Herminjard, and C. Depeursinge, "Submicrometer optical tomography by multiple-wavelength digital holographic microscopy," *Appl. Opt.* **45**(32), pp. 8209–8217, 2006.
20. B. E. Saleh and M. C. Teich, *Fundamentals of Photonics*, John Wiley and Sons, INC, New York, 1991.